Journal of Polymer Science

WILEY

JOURNAL OF POLYMER SCIENCE

RESEARCH ARTICLE OPEN ACCESS

Interplay Between the Conductivity of Polymer-Brush Functionalized Core-Shell Particles and Their Enzyme Loading Efficiency and Activity

Hongtao Cai[1] | Anila Antony[1] | Anne Linhardt[1] | Petr Formánek[2] | Leonid Ionov[3] | Alla Synytska[1]

[1]Functional Polymer Interfaces Group, Bayerisches Polymerinstitut (BPI), Universität Bayreuth, Bayreuth, Germany | [2]Leibniz-Institut für Polymerforschung Dresden e. V., Dresden, Germany | [3]Biofabrication, Universität Bayreuth, Bayreuth, Germany

Correspondence: Alla Synytska (alla.synytska@uni-bayreuth.de)

Received: 15 January 2025 | **Revised:** 7 July 2025 | **Accepted:** 9 July 2025

Funding: This work was supported by BMBF, FKZ: 031B1118B; DFG, SY 125/15-1.

Keywords: conductive core-shell particles | enzyme immobilization | laccase | polymer brush

ABSTRACT

Polymer brush-modified core-shell particles are already known as good carriers for enzymes, which can improve enzyme activity and stability compared to free enzymes[1]. However, for application in electrochemical biosensors, electron transfer between the electrode and immobilized enzyme is important. To achieve this, the materials used should combine the high enzyme loading of the polymer brush-modified particles with reasonable conductivity. In this work, two different approaches to introduce conductivity and high enzyme loading into polymer brush functionalized hybrid particles are pursued. In the first approach, conductive nanoparticles (Ag and Au) and enzymes were incorporated into poly(2(dimethylamino)ethyl methacrylate) brush shells on silica particle cores. In the second approach, conductive Ag particles were synthesized (as a core material), then grafted with PDMAEMA brush shell and afterwards loaded with enzymes. Polymer grafting density, polymer chain length, as well as the position of the conductive component either in the core or in the shell of hybrid particles showed an influence on the final particles' conductivity and loading enzyme (*Laccase* from *Trametes versicolor*) capacities. This fundamental study clarifies an interplay between the conductivity of polymer-brush functionalized core-shell particles and their enzyme loading efficiency and catalytic activity.

1 | Introduction

Enzymes have huge application perspectives in environmental monitoring and application in electrochemical biosensors, due to their high specificity and sensitivity. However, it is challenging to maintain activity as well as stability of free enzymes for a long time. Thus, enzyme immobilization on a carrier to protect the enzyme from denaturation is of high interest. Moreover, for applications in electrochemical biosensing, these carriers should combine conductivity to enable electron transfer from the active center of the enzyme to the working electrode with high enzyme loading capacity. Hybrid core-shell particles have attracted great attention for enzyme immobilization and for the design of novel highly sensitive biosensors due to their unique physical and chemical properties [1, 2], including their high surface area [3], high stability [4], high chemical catalytic activity [5] and the ability to be easily functionalized, making them suitable materials for potential applications as carrier or as sensor [1b, 6]. Polymers and inorganic particles can be combined through surface modification techniques like grafting from or grafting to [7]. By adjusting the type of a shell polymer, properties of the particle-based systems, such as adhesion [8], hydrophilicity/hydrophobicity [9], enzyme loading capacity [1a] and electron transfer [10] can be controlled with regard to

the desired application. Consequently, a variety of functions on hybrid particles through targeted polymer modification can be achieved.

During the last decade, many kinds of hybrid core-shell particles have been designed and different cores and polymers were used (SiO_2@PDMAEMA [1b], Au@PVP [11], Fe_3O_4@PEGDMA [12]). With the choice of polymer, biocompatibility and stimuli-responsive behavior could be achieved. Furthermore, core-shell particles with a conductive component have also been explored for biosensor applications [13]. For example, core-shell particles with a gold core and a conducting polymer shell have been used to develop a biosensor for the detection of dopamine [14]. The conducting polymer shell enhances the sensitivity and stability of the biosensor, while the gold core provides excellent electron transfer [14]. Overall, biosensors based on core-shell particles offer several advantages, including high sensitivity, selectivity, and stability, making them a promising candidate for a range of diagnostic and analytical applications [15]. However, most biosensors directly conjugated enzymes to the surface of conductive nanoparticles through chemical bonds [16] or directly added conductive polymers to enhance the electron transfer of the system [13c]. This leads mainly to two drawbacks. First, covalent immobilization of enzymes reduces the enzyme activity due to denaturation or conformational changes of the enzyme, and the number of enzymes immobilized is low due to the limitation of surface area [17]. Secondly, there are limitations in the long-term stability of the achieved sensors. In contrast, the immobilization of enzymes in polymer brushes can improve the long-term stability of the enzyme and thus the entire sensor system [18]. Compared to conventional enzyme immobilization strategies for electrochemical biosensing that rely on direct attachment to conductive surfaces, the use of polymer brushes offers a hydrated and spatially tunable microenvironment that can better preserve enzymatic structure and activity. Moreover, due to the modular structure of the systems presented, they also offer targeted customization with regard to the planned application.

With regard to applications in electrochemical biosensors, it is of high interest to prepare hybrid core-shell particle systems combining conductivity, high enzyme loading, and long-term enzymatic stability. This can be achieved with functional polymers for enzyme loading and protection combined with conductive material. This novel combination of materials can improve the performance and versatility of electrochemical sensors, making them more suitable for a range of applications.

In this work, different approaches to introduce conductivity as well as high enzyme loading into polymer brush functionalized particles are analyzed in detail. A series of core-shell hybrid particles, which can simultaneously protect enzymes and act as mediators between the enzyme and electrode, are presented. In order to introduce conductivity to our already well-studied SiO_2@PDMAEMA (silica particles with poly(2dimethylaminoethyl methacrylate) brush shell) system [1], conductive nanoparticles were incorporated into the polymer shell. Considering that the conductive nanoparticles in the brush may affect the immobilization of enzymes, we introduced conductivity also by using a conductive Ag particle as a core and varied polymer shell thickness and grafting density to generate particles with a patchy polymer shell, to keep the conductivity of the core material accessible. In total, two main systems with the conductive component either in the particle shell or core are investigated, and the position of the conductive components as well as their influence on the resulting conductivity and enzyme loading efficiency are discussed throughout this article. The enzyme immobilization was investigated with *laccase from Trametes versicolor* (TvL) and ABTS Assay (2,2azinobis3ethylbenzothiazoline6sulphonic acid). Laccases are multi-copper oxidases that catalyze the one-electron oxidation of a broad range of phenolic and aromatic compounds, including ABTS, while reducing molecular oxygen to water. These enzymes operate under mild conditions without requiring cofactors and are widely used in applications such as dye decolorization, wastewater treatment, and biosensing. The specific laccase used in this study, from Trametes versicolor (TvL), is commercially available, well-characterized, and stable in mildly acidic environments. Due to its high catalytic efficiency and broad substrate scope, TvL was chosen as an ideal model system. It serves as a representative for other enzymes suitable for biosensing.

Finally, this study clarifies the relationship between the introduction of conductivity and resulting catalytic activity and provides a good basis for further preparation of an electrochemical biosensor.

The particle library of the synthesized and discussed particle systems is summarized in Figure 1 including abbreviations used in this article.

2 | Results and Discussion

As the first approach to introduce conductivity to our already well studied SiO_2@PDMAEMA particle systems with high loading efficiency for TvL, silver and gold nanoparticles were incorporated into the polymer brush. Therefore, PDMAEMA was grafted via SIATRP from silica particles with 200 nm in diameter [1]. The polymer shell thickness was varied by reaction time (6 and 12 min) and could be calculated from thermogravimetric analysis (TGA). The obtained particles with polymer shell thickness of 3 and 7 nm were used for in situ generation of conductive nanoparticles in the polymer brush. Detailed characterization of polymer brush was done via TGA, dynamic light scattering (DLS) and electrophoresis measurements (zeta potential) as shown in Supporting Information (Figures S1 and S2). As illustrated in Figure 2I.a–e, SiO_2@PDMAEMA@Ag core shell particles were prepared by in situ reduction of silver nitrate on the PDMAEMA brushes [19]. SiO_2@PDMAEMA@Au was synthesized using the same method by replacing silver nitrate with chloroauric acid. To find the appropriate concentration for the reduction of silver ions in the brush, five variations with varied concentration of silver nitrate were tested. Finally, 80 mM showed the best result with a high number of silver particles and best uniformity in size visible via electron microscopy investigation (Figure S3). Lower concentrations lead to a very low amount of silver particles and higher concentrations to large and inhomogeneous particles in the polymer shell. Moreover, at higher

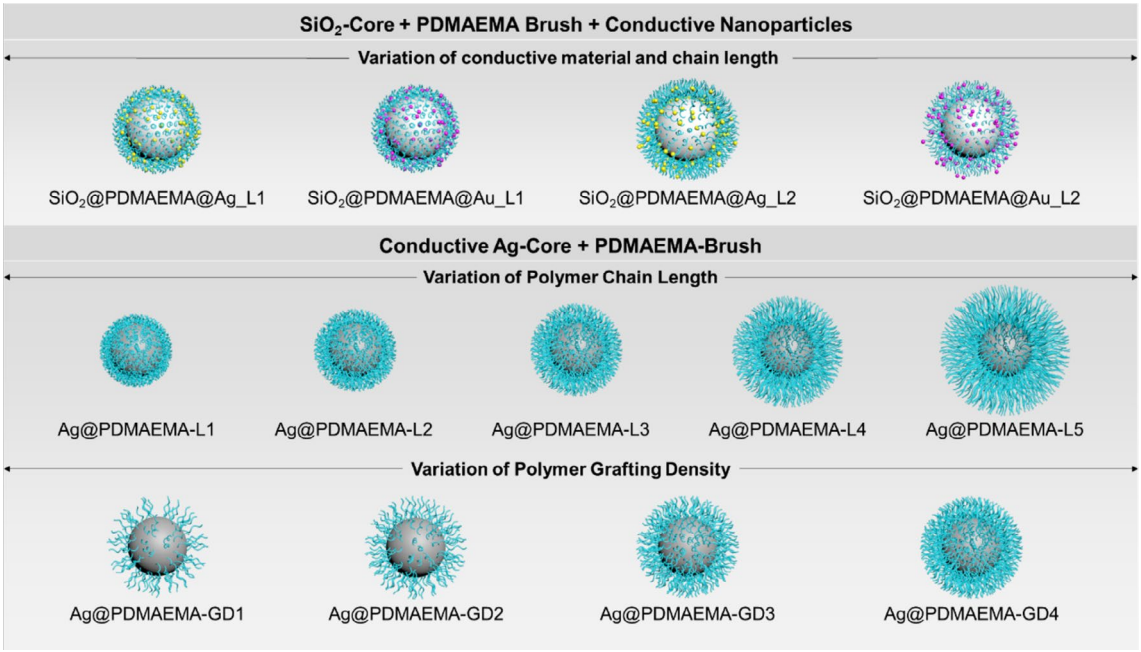

FIGURE 1 | Overview of the investigated hybrid core-shell particle systems with variation of the location of the conductive component in SiO_2-PDMAEMA (Ag_L1, Au_L1, Ag_L2, Au_L2) particle systems, the variation of polymer chain length (L1–L5) and polymer grafting density (GD1–GD4) in Ag-PDMAEMA particle systems.

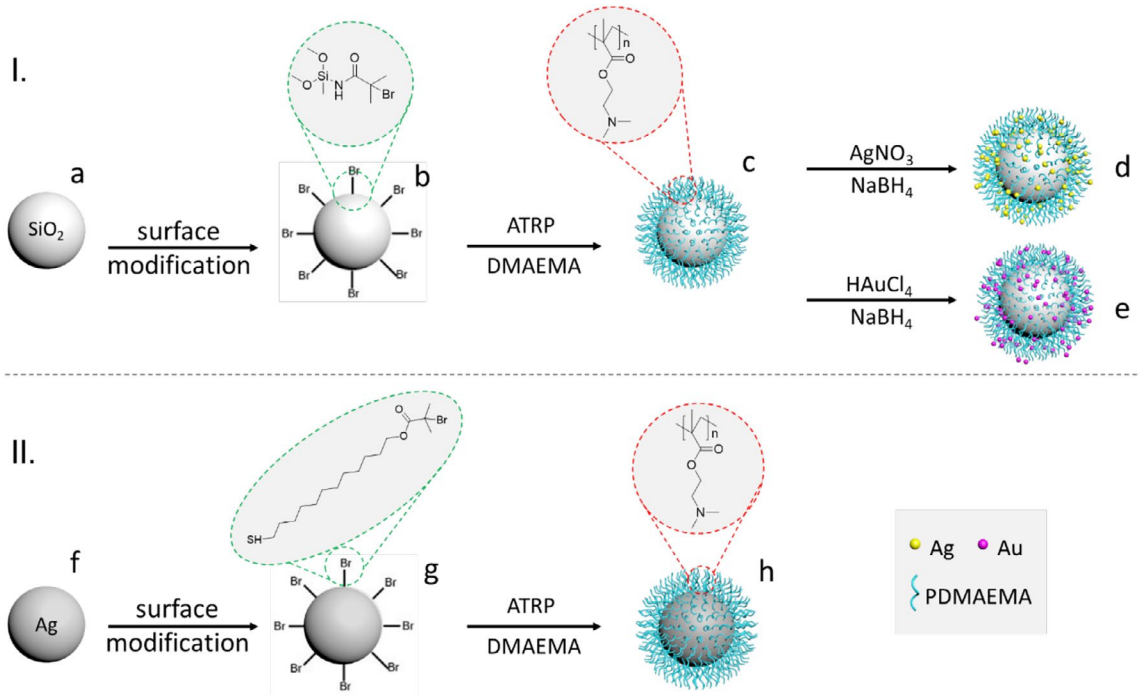

FIGURE 2 | Schematic overview over synthesis routes: I. Silica based systems: (a) SiO_2-particle (b) SiO_2-particle with bromo-initiator groups (c) SiO_2@PDMAEMA core shell particles, (d) SiO_2@PDMAEMA@Ag on the shell particles, (e) SiO_2@PDMAEMA@Au on the shell particles, II. Silver based systems: (f) Ag-particle, (g) Ag-particle with initiator groups, (h) Ag@PDMAEMA. PDMAEMA is grafted via SI-ATRP from the Br-modified particle cores (b + g).

concentrations, the metal particles start to aggregate and from large sediments in the solution. Thus, adsorption on the surface of the polymer brush was hard to achieve. The in situ generation of gold nanoparticles in the polymer shell led to comparable results (Figure S4). The results obtained indicate also 80 mM chloroauric acid as an optimal concentration. SEM and TEM and cryo-TEM were used to study the surface morphology and shape of the generated particles.

As shown in Figure 3a, SiO_2 native has perfect spherical shape and smooth surface. The surface remains smooth after polymer grafting, but bridging by polymers between

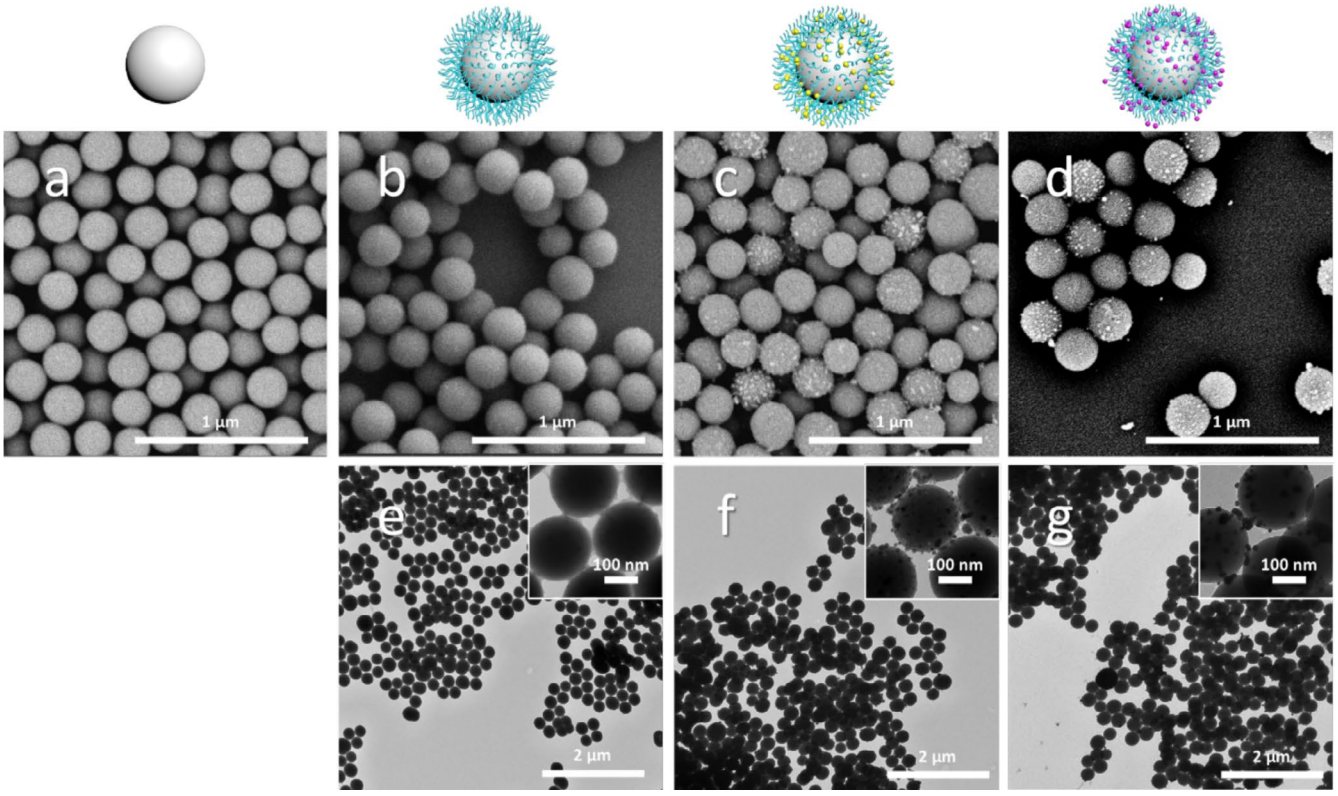

FIGURE 3 | SEM images of: (a) native SiO_2 particle, (b) SiO_2@PDMAEMA_L2, (c) SiO_2@PDMAEMA@Ag_L2, (d) SiO_2@PDMAEMA@Au_L2 and TEM images of (e) SiO_2@PDMAEMA_L2, (f) SiO_2@PDMAEMA@Ag_L2 and (g) SiO_2@PDMAEMA@Au_L2 core shell particles.

the particles can be observed, indicating successful polymerization (Figure 3b, exemplary shown for particles with 7 nm polymer shell thickness). After in situ growing silver and gold nanoparticles, in SEM bright spots are visible on the particle surface (Figure 3c and Figure 3d). Successful incorporation of Ag and Au nanoparticles in the polymer shell could be further proved by TEM (Figure 3e–g). However, not every particle shows a perfect in situ metal functionalization due to the uncontrolled reduction process, but it is possible to reach small metal particles on the polymer shell with low concentrations of chloroauric acid or silver nitrate, due to the fast sodium borohydride reduction. Unfortunately, the resulting particle systems show decreased dispersibility compared to systems without conductive particles on the polymer brush. It is assumed that the particles shield the charge of the PDMAEMA brush, resulting in higher hydrophobicity as well as a greater tendency to agglomerate.

To investigate the resulting conductivity of these hybrid particles, resistivity was measured of the resulting composite particles by four-point test measurement and the corresponding conductivity was calculated. Unfortunately, the obtained conductivity of all systems tested is very low but could be improved by 7 orders of magnitude compared to the SiO_2@PDMAEMA particles (Figure 4). To determine the enzyme activity of the obtained particles, TvL was used as an enzyme, and activity was investigated by photometrical ABTS assay measurements. Polymer brushes with a thickness of 7 nm exhibit much higher enzyme activity per particle than those with a thickness of 3 nm. With the introduction of conductive nanoparticles in the polymer brush, the good enzyme loading efficiency achieved for SiO_2@PDMAEMA_L2 decreased. It seems that the loading capacity decreases as the intended places for enzymes are already occupied by the conductive particles (Figure 4). For PDMAEMA@Au, higher enzymatic activity was achieved compared to PDMAEMA@Ag for short polymer brushes (3 nm). In contrast, for longer brushes (7 nm thickness), the enzymatic activity of both systems was low and quite similar. It is assumed that in short brushes, the enzyme interacts more directly with the nanoparticle surface due to less steric and diffusion limitations. Moreover, gold is known to have better biocompatibility and may promote better enzyme orientation or less denaturation, and it has already been reported to increase the laccase activity, particularly at acidic and near-neutral pH levels [20]. This can result in higher retained activity of enzymes immobilized together with Au compared to Ag nanoparticles.

In summary, conductivity could be improved significantly for these particle systems; however, enzyme loading was low. An increase in polymer shell thickness could help to improve enzyme activity per particle and thus loading efficiency as well as dispersibility, but probably without a sufficient increase in conductivity. Moreover, these particle systems show drawbacks in stability since the conductive particles are immobilized by physical interactions with the polymer brush, leading to difficulties during further processing, for example, the washing procedure of the particles and buffer exchange by sonication and centrifugation right before enzyme immobilization.

Due to the inhomogeneous in situ growth of nanoparticles on our hybrid systems, the low stability due to low physical bonding

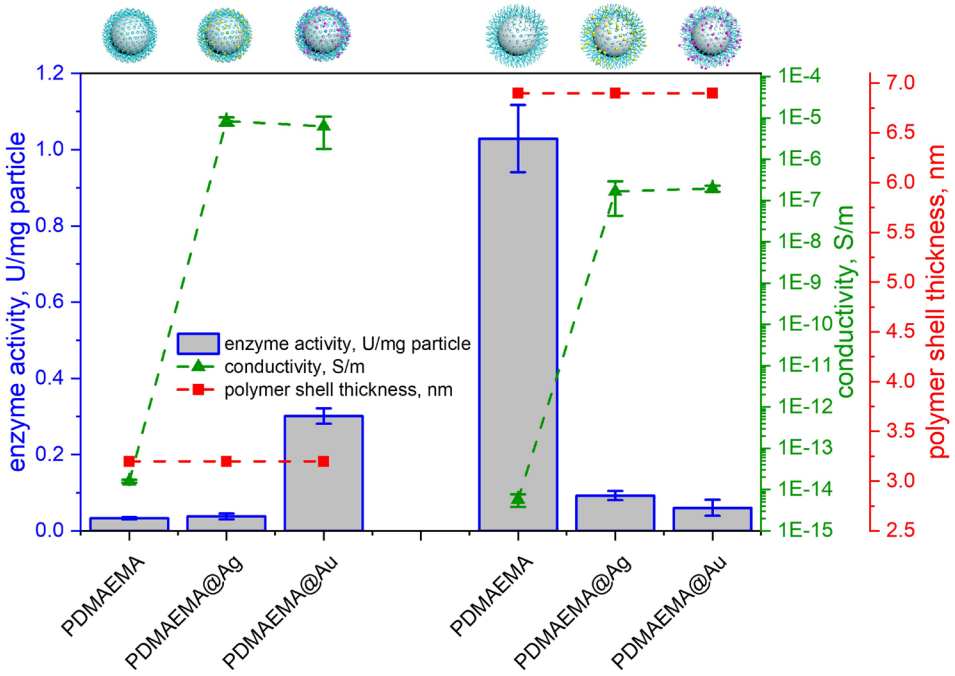

FIGURE 4 | Activity of loaded enzyme per particle, polymer shell thickness as well as conductivity of the synthesized core-shell particles. *Error bars represent standard deviation from three independent experiments.

of nanoparticles to the polymer brush, the loss of dispersibility as well as low enzyme activity per particle and low conductivity, the strategy was changed, and conductive Ag particles were directly modified with polymer brushes. This technique shows various advantages. First, direct surface modification helps to increase the hydrophilicity of hydrophobic silver particles and leads to well-dispersed particles which are of high importance for further modification with enzymes. Second, the conductivity of the system can be controlled through the thickness as well as grafting density of the polymer brush. Additionally, the enzyme loading capacity of the polymer brush is not influenced by immobilized conductive particles, and the resulting particles show sufficient robustness for further processing.

First, silver particles were synthesized by kinetically controlled seeded growth [21]. Since the reduction process of silver is very rapid, uniform large-sized spherical particles are hard to achieve. However, by reducing the concentration of the seed solution, silver particles with acceptable dispersity could be obtained. For grafting of the polymer brush, SI-ATRP (Surface-initiated atom transfer radical polymerization) was used to graft PDMAEMA from the initiator-modified particle surface (Figure 2f–h) as already shown for silica-based systems. SI-ATRP allows easy variation of polymer grafting density by the ratio of Br-initiator and "dummy-initiator". To introduce bromine functional groups to the Ag particle surface (Br-initiator), 11Sulfanylundecyl 2bromo2methylpropanoate- was used. For variation of grafting density, 2-mercaptoethanol was added as "dummy-initiator" [1]. The choice of 2-mercaptoethanol was made due to its low molecular weight and hydrophilicity. In addition to varying the grafting density, steric hindrances and reduced surface accessibility caused by the dummy initiator can be avoided due to its low molecular weight, and at the same time, a favorable hydrophilic environment can be created, which facilitates the immobilization of enzyme and dispersibility of the whole system.

In this study, Brinitiator amounts of 10%, 25%, 50%, and 100% were investigated. Moreover, five systems with DMAEMA monomer concentrations of 0.28, 0.99, 1.7, 2.2, and 2.6 M were synthesized to tune the polymer chain length and to find suitable conditions and balance of conductivity and enzyme loading efficiency. As shown in Figure 5a, silver particles with polygonal shapes and a diameter of ~170 nm (calculated from SEM, Figure S5) were successfully synthesized. DLS shows a narrow size distribution with a hydrodynamic diameter of 190 nm. The success of the polymerization on particles was proven by SEM, cryo-TEM, TGA, DLS, and electrophoresis measurements. After grafting of PDMAEMA brushes, the surface morphology gradually becomes smoother with increasing grafting density or monomer concentration (Figures 5 and 6), due to an increase in polymer brush thickness, making the edges and corners of the particles less clear. The cryo-TEM images also show an increase in polymer shell thickness with increasing monomer concentration as well as an increasing amount of surface initiator (exemplarily shown for particles with variation of grafting density, Figure 6). This was also proved by TGA. With the increase in monomer concentration or amount of surface initiator, the weight loss of the sample also increases (Figure 7a). TGA also allows the calculation of the amount of polymer on the particle surface and the polymer shell thickness (dry state). Since the particle morphology is close to spherical particles, the previously published equation [22] was used to calculate the approximate thickness of the polymer brush. The calculated results are summarized in Table 1.

The obtained particles were further characterized concerning their hydrodynamic diameter, swelling properties, and electrokinetic potential (Figure S6). As expected, the DLS

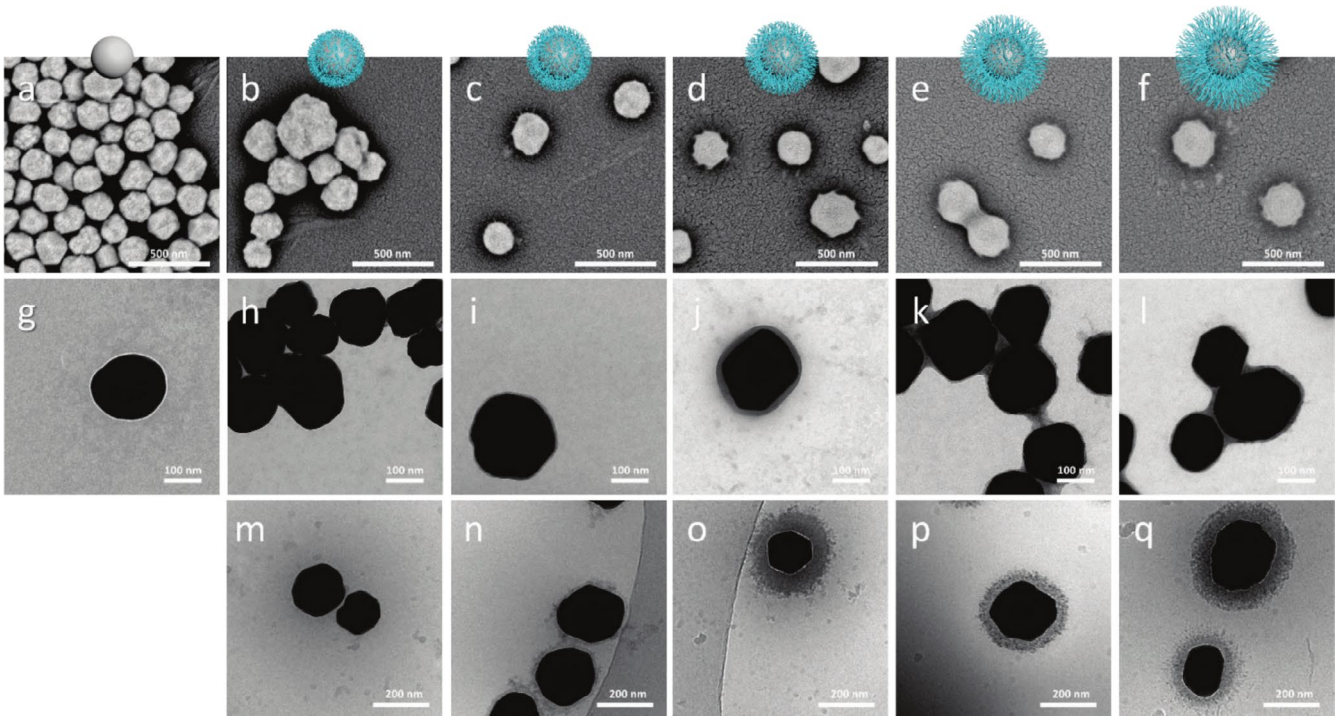

FIGURE 5 | SEM images of native Ag particles (a), Ag@PDMAEMA_L1 (b), Ag@PDMAEMA_L2 (c), Ag@PDMAEMA_L3 (d), Ag@PDMAEMA_L4 (e), Ag@PDMAEMA_L5 (f), and TEM images of native Ag particles (g), Ag@PDMAEMA_L1 (h), Ag@PDMAEMA_L2 (i), Ag@PDMAEMA_L3 (j), Ag@PDMAEMA_L4 (k), Ag@PDMAEMA_L5 (l), and Cryo-TEM images of Ag@PDMAEMA_L1 (m), Ag@PDMAEMA_L2 (n), Ag@PDMAEMA_L3 (o), Ag@PDMAEMA_L4 (p), Ag@PDMAEMA_L5 (q). Increase in shell thickness with longer chain length can be observed.

analyses show that with increasing monomer concentration or number of Br-initiator groups, the hydrodynamic radius of the particles also increases (Figure 7b). However, this observed increase in hydrodynamic size cannot solely be attributed to the increasing brush thickness grafting density. Partial particle aggregation may also occur in aqueous media, especially considering the high molecular weight and moderate grafting density of the PDMAEMA brushes. These factors, together with the high density of silver nanoparticles, may lead to transient aggregation and biased DLS measurements due to the sixth-power scattering dependence on particle size. Nevertheless, the DLS shows the expected trend and also demonstrates the good swelling properties of the systems presented in aqueous solutions. The surface isoelectric point of the silver particles moved from pH 3 to pH values around 9 after grafting the polymer (Figure 7c,d). All Ag@PDMAEMA particles show a positive surface potential (about 40 mV) at pH 4, which provides the favorable conditions for TvL immobilization [1a, 23].

Due to the linear correlation between monomer concentration and polymer shell thickness, the polymer shells with 3, 11, 23, 35, and 41 nm (calculated from TGA results) could be grafted onto silver particles with a core hydrodynamic diameter of ~190 nm and used for enzyme immobilization experiments. For comparison, enzyme immobilization and ABTS assay measurements were also tested with the native Ag particles without polymer brush, leading to no detectable catalytic activity. With increasing thickness of the polymer brush, the catalytic activity per particle and the immobilization efficiency increase, reaching a plateau at a shell thickness of 23 nm (Figure 8d). The catalytic activity per polymer and enzyme decreases with higher chain length. Moreover, TGA analysis shows a constant increase in weight after enzyme immobilization for all samples and slightly higher values for the highest polymer shell thickness (Figure 7a). These observations can be explained by different effects. On the one hand, steric hindrance in areas close to the particle core as well as polymer entanglements in the areas with higher distance to the particle core (Figure 8b) affect enzyme loading for higher chain length. This occurs due to the different behavior of brushes grafted to curved surfaces compared to flat surfaces. Brushes grafted to the curved surface of a spherical particle also undergo a transition from mushroom to semi-diluted (SDPB) to concentrated (CPB) conformation with increasing grafting density, like brushes on flat surfaces, but the crowding from the polymers decreases away from the particle surface due to the curvature [24] (Figure 8a,b). Furthermore, large amounts of polymer can hinder the substrate ABTS from reaching the immobilized enzymes or the immobilized enzymes lose activity. If this is the case, inactive or not reacting but immobilized enzymes will contribute to the enzyme mass fraction determined by TGA but show no activity during ABTS assay measurement. The fact that the catalytic activity per enzyme (U/mg enzyme) also decreases for higher polymer shell thickness confirms this hypothesis.

With higher grafting densities, the catalytic activity per particle and enzyme immobilization efficiency increase as well. Thus, enzyme loading is more efficient with increasing amounts of polymer per particle (Figure 8e). Interestingly, the catalytic activity per polymer is higher for low grafting

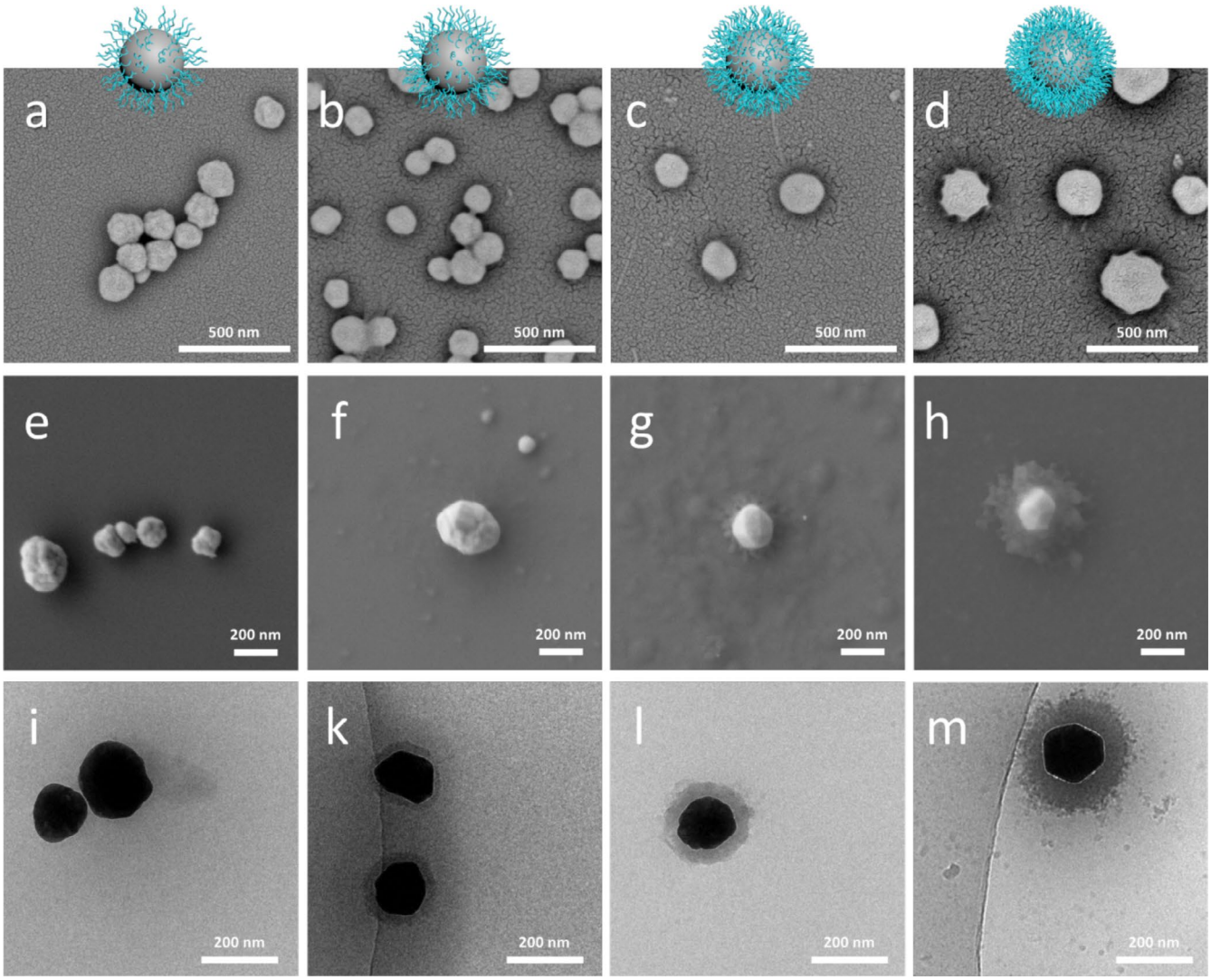

FIGURE 6 | SEM images of Ag@PDMAEMA_GD1 (a + e), Ag@PDMAEMA_GD2 (b + f), Ag@PDMAEMA_GD3 (c + g) and Ag@PDMAEMA_GD4 (d + h), and Cryo-TEM images of Ag@PDMAEMA_GD1 (i), Ag@PDMAEMA_GD2 (k), Ag@PDMAEMA_GD3 (l) and Ag@PDMAEMA_GD4 (m).

density. This can be attributed to a higher distance and thus reduced steric hindrance due to the formation of mushroom-like polymer structures, which facilitates enzyme immobilization and enables more efficient use of the available polymer chains. Furthermore, enhanced diffusion of the ABTS substrate within less crowded brushes may also contribute to this effect.

The initial activity of TvL was 0.34 ± 0.09 U/mg. Interestingly, this is increased significantly for all hybrid systems, with the best result for Ag@PDMAEA_L3 with 14.95 U/mg enzyme calculated from the ABTS assay and TGA results. One explanation is that the TvL was used as received without further purification. The enzyme used was not obtained with a high degree of purity, which is also reflected in its low activity per mass. As several washing steps are carried out after the incubation of the hybrid particles in TvL solution, purification from impurities takes place simultaneously, which leads to higher specific activities since all impurities not interacting with the polymer brush are removed during the washing procedure.

Enzyme immobilization and its effect on the hybrid particle size as well as surface charge were also investigated by DLS and electrokinetical potential, respectively. There is no significant change in hydrodynamic diameter after enzyme immobilization, probably due to collapse of the brush-like structure of the polymer shell after immobilization and thus less swelling due to electrostatic interactions between polymer and enzyme, which is also indicated by decrease in IEP value after enzyme immobilization (Figure 7b–d).

With respect to conductivity, short polymer brushes as well as low grafting densities give the best results, since the Ag surface remains accessible in this type of particle, due to their unique patchy character. With increase in polymer brush thickness, the conductivity of the hybrid Ag particles decreases to very low values (Figure 9). Thus, enzyme loading and conductivity are in a competitive relationship. Nevertheless, we could improve the conductivity of the systems compared to silica-based systems. Moreover, stability studies in acetate buffer solution (pH 4, stored at 5°C ± 1°C, see Figure S8) solution show also an improved stability compared to free laccase stored under the same conditions.

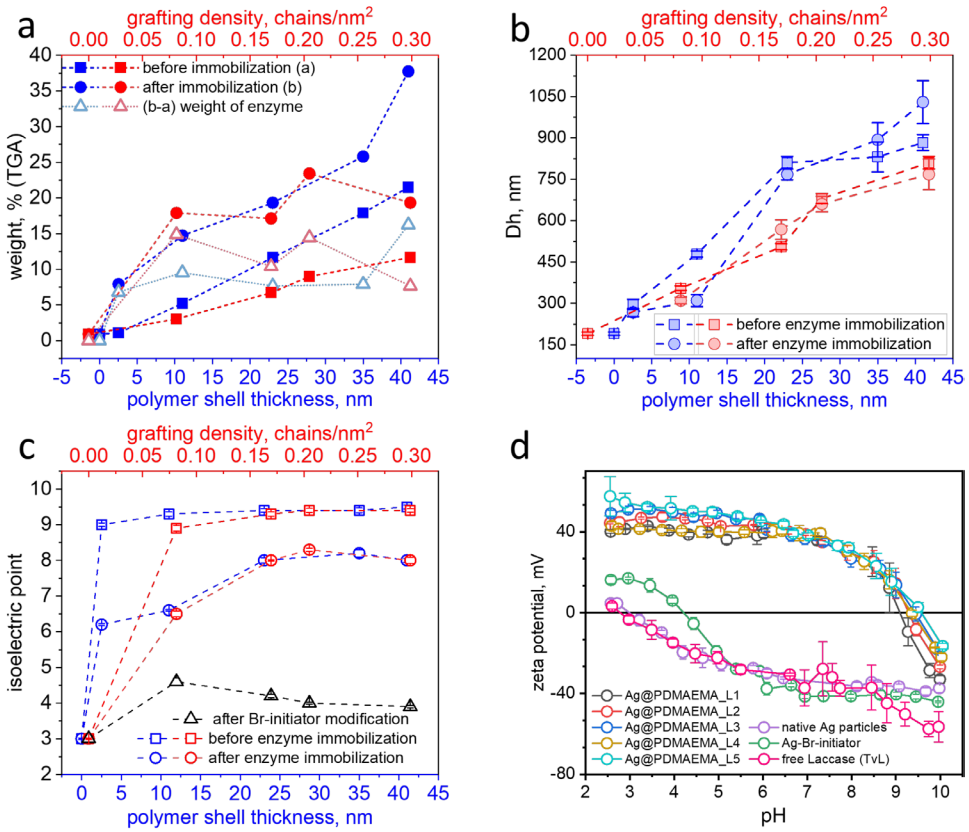

FIGURE 7 | Estimated organic mass fraction (including polymer and enzyme components) determined by TGA (a) hydrodynamic radius (b; $n = 3$), isoelectric point (c; $n = 3$) of the Ag@PDMAEMA based particles with different polymer shell thickness (blue) and grafting density (red) before (■) and after (●) enzyme immobilization. Change in zetapotential (d) for Ag@PDMAEMA_L1-L5, native Ag particles, Ag particles with Br-Initiator and free TvL.

3 | Conclusion

In conclusion, a library of hybrid core-shell particles was synthesized, incorporating a PDMAEMA polymer brush and a conductive component (Ag or Au) located either in the polymer shell or as a core material. Following that, a comparison was made of the achieved enzyme activities and conductivity of the resulting system. It was demonstrated that the placement of a conductive particle into the core, as opposed to the immobilization of conductive particles within the brush-like polymer shell, resulted in particles with enhanced conductivity, stability, dispersibility, and good enzyme loading efficiency.

Also, the impact of grafting density and polymer shell thickness in the conductive core-shell Ag(core)-PDMEMA (shell) particles was investigated. The properties of the polymer brush were controlled and varied by different monomer concentrations and different ratios of "dummy initiator" and bromosurface-initiator. The enzyme immobilization efficiency and resulting catalytic activity per particle increased with increasing polymer fraction of the hybrid particle system up to 1.15 ± 0.14 U/mg particle for high grafting density (0.3 polymer chains/nm^2) and 1.23 ± 0.07 U/mg particle for 35 nm polymer shell thickness. However, the highest conductivity (0.004 ± 0.001 S/m) was achieved with short polymer brush (3 nm) as well as low grafting density (0.08 polymer chains/nm^2), since the core Ag particle material was accessible. Furthermore, hybrid core-shell Ag(core)-PDMEMA (shell) particles demonstrated excellent water dispersibility and stability, which renders them highly suitable for application in detection and catalytic reactions.

As a proof of concept, it has been demonstrated that laccase immobilized in the polymer brush layer retains catalytic activity toward ABTS oxidation, as confirmed via UV–Vis absorbance assays. In an electrochemical biosensing context, this redox reaction could be transduced into a measurable electrochemical current signal, provided that the conductive silver core establishes an electron transfer pathway to an electrode surface. Although a full biosensing or catalytic assay falls beyond the presented scope, we propose a proof-of-concept sensing model, where the immobilized enzyme (e.g., laccase) catalyzes redox reactions (e.g., ABTS oxidation), and the conductive core could serve as a transducing element in an electrochemical sensor (Figure S9).

4 | Materials and Methods

4.1 | Materials

Tetraethyl orthosilicate (TEOS, Sigma, 99%), ammonia solution (NH_4OH, Sigma, 28%–30% solution), ethanol abs. (EtOH, Sigma, 99.9%), copper(II) bromide ($CuBr_2$, Sigma, 99.999%), (3-aminopropyl)triethoxysilane (APTES, Sigma, 99%), a-bromoisobutyryl bromide (Br-initiator for SiO_2-particles) Sigma, 98%), propionyl bromide (Sigma, 97%),

TABLE 1 | Characterization summary of analyzed particle systems.

Sample ID	D_h (nm)^{DLS} ($n=3$)	c(DMAEMA), mol/L	Grafting density, chains/nm^2 (TGA, GPC)	Br-initiator/ dummy initiator	Shell thickness, nm^{TGA}	Zetapotential at pH 4, mV	IEP, pH ($n=3$)
SiO_2	227 ± 10			1:1	—	−53 ± 0.8	< 3
SiO_2@ PDMAEMA_L1	350 ± 15	2.9[a]			3	40 ± 0.6	9.1 ± 0.08
SiO_2@ PDMAEMA_ L2	428 ± 22	2.9[a]			7	38 ± 0.9	9.5 ± 0.1
SiO_2@ PDMAEMA@ Ag_L1	358 ± 18	2.9[a]			3	36 ± 1.8	9.0 ± 0.06
SiO_2@P@ AgPDMAEMA_ L2	416 ± 28	2.9[a]			7	36 ± 0.7	9.3 ± 0.03
SiO_2@ PDMAEMA@ Au_L1	345 ± 13	2.9[a]			3	43 ± 0.7	9.0 ± 0.05
SiO_2@ PDMAEMA@ Au_L2	440 ± 25	2.9[a]			7	42 ± 1.5	9.3 ± 0.06
Ag	190 ± 6				—	−11 ± 0.3	3.0 ± 0.02
Ag@ PDMAEMA_L1	296 ± 19	0.28	0.30[b]	1:0	3	39 ± 1.1	9.0 ± 0.05
Ag@ PDMAEMA_L2	479 ± 11	0.99			11	46 ± 0.6	9.3 ± 0.06
Ag@ PDMAEMA_L3	810 ± 23	1.70			23	49 ± 2.1	9.4 ± 0.05
Ag@ PDMAEMA_L4	831 ± 54	2.20			35	41 ± 3.0	9.4 ± 0.07
Ag@ PDMAEMA_L5	883 ± 29	2.60			41	52 ± 1.5	9.5 ± 0.06
Ag@ PDMAEMA_GD1	360 ± 8	1.70	0.08	1:9	7	58 ± 2.7	8.9 ± 0.08
Ag@ PDMAEMA_GD2	511 ± 11	1.70	0.17	1:3	14	56 ± 3.1	9.3 ± 0.06
Ag@ PDMAEMA_GD3	683 ± 18	1.70	0.21	1:1	18	47 ± 1.8	9.4 ± 0.06
Ag@ PDMAEMA_GD4	810 ± 23	1.70	0.30	1:0	23	49 ± 2.1	9.4 ± 0.05

[a]Variation of chain length done by time variation during polymerization (6 min for L1 and 12 min for L2).
[b]The same batch of surface-modified particles was used.

tris(2-pyridylmethyl)amine (TPMA, Sigma, 98%), tin(II) 2-ethylhexanoate (Sigma, 95%), ethyl a-bromoisobutyrate (EBiB, Sigma, 98%), silver nitrate (Sigma, ≥99.0%), 2-Mercaptoethanol(Sigma, ≥99.0%), 11Mercaptoundecyl 2-Bromo-2-methylpropanoate (Br-initiator for Ag-particles, TCI, >95.0%), dopamine hydrochloride (Sigma, >98.0%), polyvinylpyrrolidone (PVP, Sigma, M_w 40,000), hydrogen tetrachloroaurate(III) trihydrate ($HAuCl_4 \cdot 3H_2O$, Acros, 99%), L-ascorbic acid (Sigma, 99%), acetonitrile (Sigma, HPLC grade ≥ 99.9%), sodium borohydride ($NaBH_4$, Sigma, 99%), dichloromethane (Acros, 99.99%), and 2,2′-azino-bis(3-ethylbenzothiazoline-6-sulfonic acid) (ABTS, Boehringer Mannheim GmbH) were used as received. 2-(Dimethylamino)ethylmethacrylate (DMAEMA, Sigma, 98%) was passed through basic, neutral, and acidic aluminum oxide columns for 20 min to remove the inhibitor prior to polymerization.

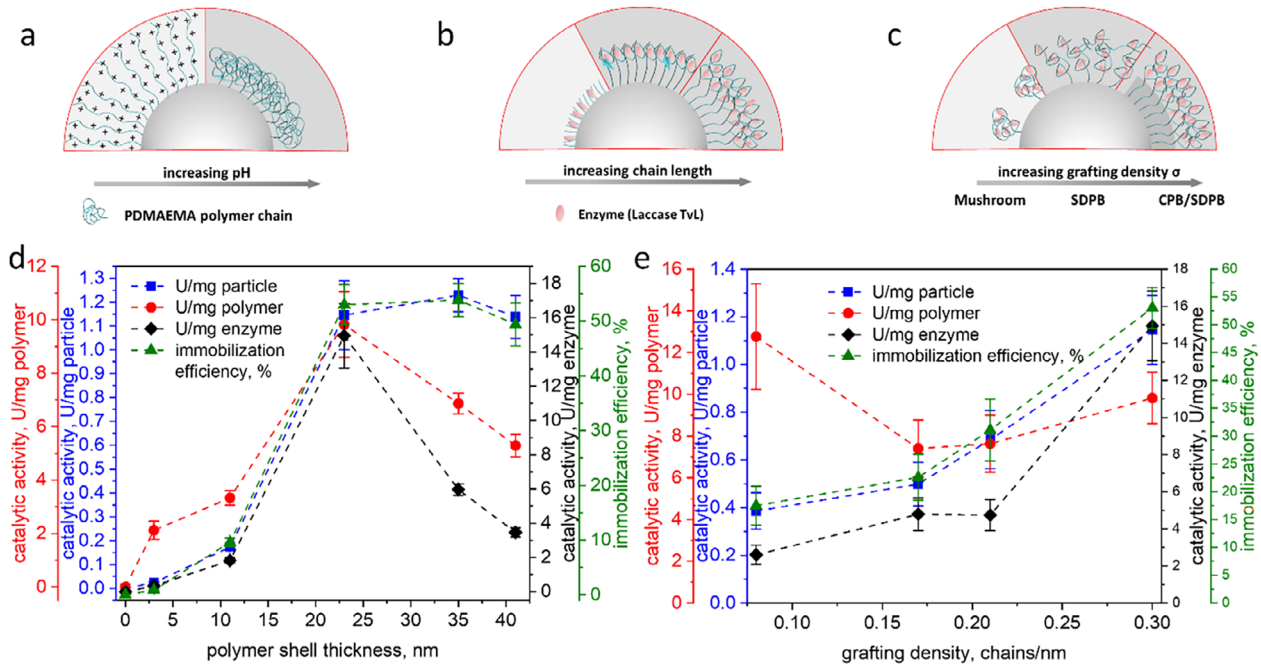

FIGURE 8 | Schematic illustration of PDMAEMA brush conformation under different conditions. (a) In aqueous solutions with low pH values the polymer chains are positively charged and show brush-like character due to electrostatic repulsion. At higher pH values the brush collapses and the PDMAEMA chains coil to a mushroom structure. In contact with enzymes, a collapse of the polymer brush is also assumed. With increase in chain length (b) and grafting density (c), the enzyme immobilization efficiency as well as catalytic activity of the resulting hybrid system (U/mg particle increases due to higher polymer fraction). It is assumed that at low grafting densities with high chain length the loading capacity of the polymer can be better utilized due to less repulsion forces between the polymer chains. At higher grafting densities repulsion forces between the polymer chains close to the polymer core as well as entanglements in the outer part of the shell occur. The catalytic activity detected with ABTS assay is compared for variation in polymer shell thickness (monomer concentration) (d) and grafting density (e) and presented as 'U/mg polymer' (red), 'U/mg particle' (blue) and 'U/mg enzyme' (enzyme). The enzyme immobilization efficiency is also presented (green).

4.2 | Scanning Electron Microscopy (SEM)

The SEM imaging of SiO_2, Ag, and composite particle systems was conducted with a VolumeScope scanning electron microscope (Thermo Fisher Scientific GmbH, Germany), operating at 3 keV, ~13 pA using a secondary electrons detector and T1 detector. For sample preparation, 2 μL of particle dispersion in water (1 mg/mL) was dropped on a hydrophilized 5 × 5 mm silicon wafer (cleaned in a 1:1:1 mixture of H_2O_2, NH_4OH and H_2O) and dried in ambient conditions. In order to enhance topography contrast, samples were coated with platinum (around 2 nm) using a Leica EM ACE 600 sputter coater (Leica Microsystems, Germany).

In addition, SEM imaging was conducted with an NEON40 (Carl Zeiss Microscopy Deutschland, Germany), operating at 2 keV, ~200 pA using a secondary electrons detector and a back-scattered electrons detector. 2 μL of quaternized particle dispersion in water (1 mg/mL) was dropped on a hydrophilized 5 × 5 mm silicon wafer and, after drying in ambient conditions, inspected in SEM (without any coating). Hydrophilization was done in air plasma at a power of 70 W for 60 s (Femto, Diener Electronic, Germany).

4.3 | Dynamic Light Scattering (DLS) and Electrokinetic Measurements

The pH-dependent electrokinetic properties of the particles were measured by Zetasizer Ultra Red from Malvern Instruments Ltd. and an MPT-3 autotitrator. 24 mg particles were dispersed in 30 mL of 10 mM KCl solution. Controlling the pH of the prepared suspension was done by adding 0.1 M KOH or 0.1 M HCl aqueous solution through a titration system. Three measurements were recorded for each sample at each pH value. The same suspensions were used for the dynamic light scattering (DLS) measurements at the same device and measured three times for each sample. Ultrasonication was applied before measurement to ensure good dispersion. The aqueous testing conditions were chosen to closely simulate the intended application environment of the enzyme-functionalized nanoparticles, which operate in aqueous buffer systems.

4.4 | Transmission Electron Microscopy (TEM) and Cryo-TEM

The TEM and cryo-TEM imaging of SiO_2, Ag, and composite particle systems was conducted with a Libra120 (Carl Zeiss Microscopy Deutschland, Germany), operating at 120 kV. For TEM, 2 μL of particle dispersion in water (1 mg/mL) was dropped on hydrophilized carbon film supported by a copper TEM grid and dried at ambient conditions. For cryo-TEM, 2 μL of particle dispersion in water (1 mg/mL) was dropped on each side of hydrophilized QUANTIFOIL R3.5/1 TEM grid, blotted for 0.2 s, and plunged in liquid ethane using Leica GP grid plunger (Leica Microsystems GmbH, Germany). Hydrophilization was done in air plasma at a power of 70 W for 20 s (Femto Plasma

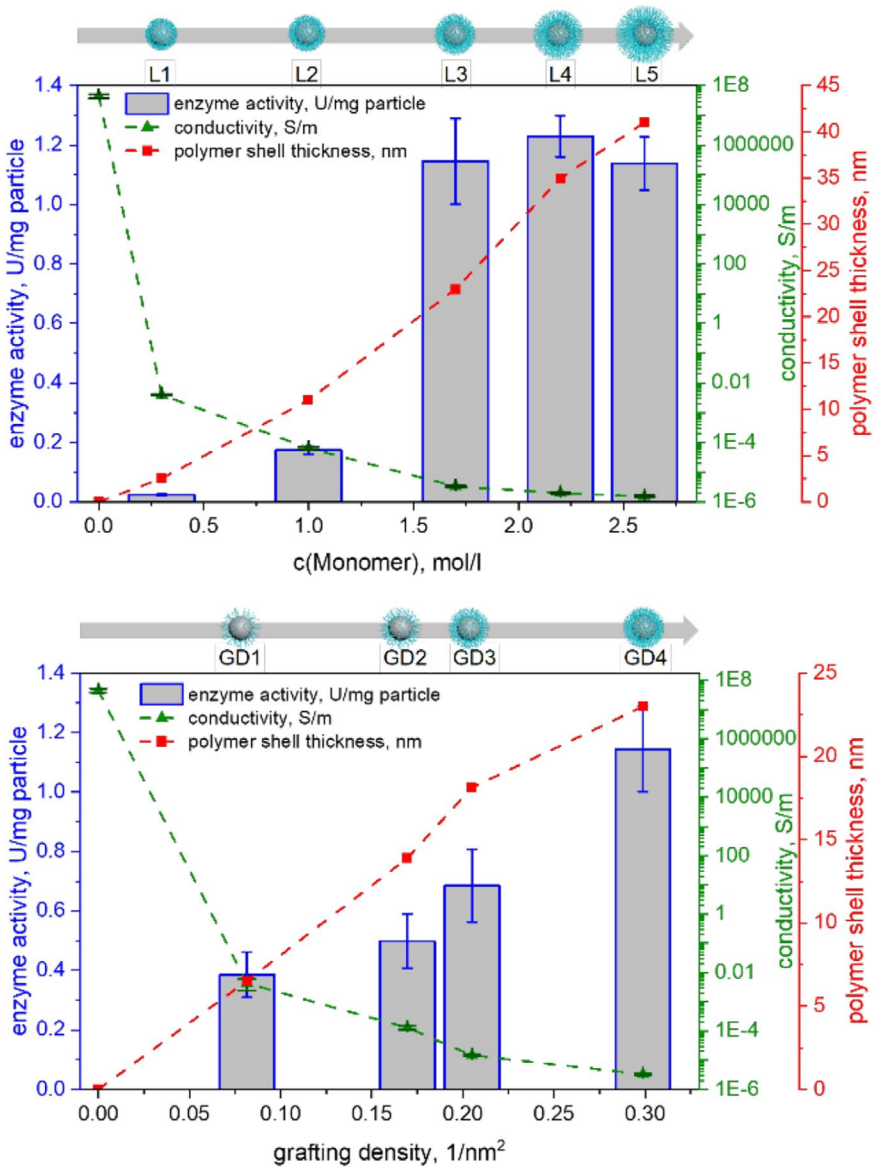

FIGURE 9 | Activity of loaded enzyme per particle (U/mg particle, $n = 3$), polymer shell thickness, as well as conductivity ($n = 3$) of the synthesized and investigated particles and the dependence on the used monomer concentration and grafting density.

Cleaner, Diener Electronic, Germany). To increase the contrast of the polymer brush, particles with PDMAEMA were stained (quaternized) with CH_3I. Therefore, 2 mL of iodomethane was added to 10 mg particles and stirred overnight. Iodomethane was removed by centrifugation and the particles redispersed in Millipore water.

4.5 | Gel Permeation Chromatography

The molecular weight of the bulk polymer obtained after precipitation was determined using GPC equipped with a HPLC-Pump 1200 Infinity (Agilent Technologies Inc., USA), an autosampler (1260 Infinity, Agilent Technologies Inc., USA) and a PolarGel-M column (100 × 7.5 mm). The flowrate was 1 mL/min, and DMAx + 3 g/L LiCl was used as eluent.

For the calculation of grafting density, the following equation was used:

$$\Gamma = \frac{R \times \rho_{Ag} \times \varphi_{\text{Polymer}} \times N_A}{3M_n \times (1 - \varphi_{\text{Polymer}})} \quad (1)$$

R is the radius of the core particle, ρ_{Ag} the density of silver, φ_{Polymer} is the polymer fraction of PDMAEMA determined by TGA analysis, N_A the Avogadro number, and M_n the molecular weight determined by GPC.

4.6 | Synthesis of SiO_2 Particles and Surface Modification

SiO_2 particles with 200 nm diameter were synthesized by Stöber method. First, to yield 100 nm SiO_2 particles, 50 mL ethanol and 3 mL NH_4OH (28%–30%) were stirred at 500 rpm for 3–4 min in a clean 500 mL snap cap vial. Afterwards, 1.5 mL of tetraethylorthosilicate (TEOS) were added dropwise. After stirring for 12 h at room temperature, 50 mL of the resulting mother solution (100 nm

SiO_2 particles) were transferred to a new vial and 350 mL ethanol and 24 mL NH_4OH (28%–30%) were added. After stirring for 3–4 min, 12 mL of TEOS were added dropwise. After stirring for 12 h at room temperature, the resulting 200 nm SiO_2 particles were isolated by centrifugation at 12000 rpm for 10 min and washed five times with ethanol and dried under vacuum at 60°C overnight.

4.7 | Functionalization of SiO_2 Particles With APTES

SiO_2 particles (2 g) were placed in a 250 mL round-bottom flask with a stir bar, then 95 mL of ethanol and 5 mL of 3-aminopropyltriethoxysilane (APTES, Sigma, 99%) were added. After stirring for 12 h at room temperature, the SiO_2-NH_2 particles were isolated by centrifugation at 12000 rpm for 10 min and washed five times with ethanol and dried under vacuum at 60°C overnight.

4.8 | Preparation of Bromo-Functionalized SiO_2

APTES-modified SiO_2 particles (1 g) were placed in a 100 mL round bottom flask with a stir bar, then 50 mL of dichloromethane (dry) was added. After stirring for 3 min, 0.5 mL of a bromoisobutyryl bromide (Br-initiator, Aldrich, 98%) and 0.36 mL of propionyl bromide (Aldrich, 97%) were added. After stirring for 3 min, 2 mL of triethylamine was added, and the resulting solution was stirred at room temperature at 700 rpm. After 2 h, the particles were collected by centrifugation at 12000 rpm for 10 min and washed two times with DCM, three times with ethanol, and dried under vacuum at 60°C overnight.

4.9 | Synthesis of Ag Particles

According to previous literature reports [21], silver particles (170 nm diameter) were synthesized in batches, using gold seeds. 5 mL of PVP (5 wt % in H_2O) and 10 μL of $HAuCl_4$ (0.25 M) were dissolved in 5 mL of H_2O. After that, 0.6 mL of $NaBH_4$ (0.1 M) was injected under vigorous stirring, giving rise to a yellowish solution of Au nanoparticles. The Au nanoparticles obtained were then aged for 6 h, allowing complete decomposition of $NaBH_4$ before serving as the seeds in the subsequent seeded growth procedure. 2 mL of PVP (5 wt % in H_2O), 1 mL of acetonitrile, and 200 μL of ascorbic acid (0.1 M) were added in 2 mL of H_2O, which was tempered to 25°C. Then, 150 μL of $AgNO_3$ (0.1 M) was added, followed by quick injection of 0.1 μL of the seed solution. After 2 h, the particles were collected by centrifugation at 4000 rpm for 20 min and washed 3 times with ethanol, redispersed in ethanol, and stored in therefrigerator.

4.10 | Grafting of PDMAEMA Using Surface-Initiated ATRP ("Grafting From")

4.10.1 | SiO_2@PDMAEMA

A total of 500 mg Br-initiator-modified silica particles, 1 mL DMAEMA, 2 mL anhydrous DMF, 0.15 μL EBIB, 30 mL $CuBr_2$ (0.1 M solution in DMF), 6.5 mg TPMA were add to a reaction-tube with a stir bar, then the tube was sealed with a rubber septum and purged with argon and sonicated (80 W) in an ice-water bath for 30 min. Afterwards, 100 mL Sn(II)2ethylhexanoate dissolved in 1 mL DMF were injected. The polymerization was carried out in oil bath at 60°C- for 6 min for shorter chains (SiO_2@PDMAEMA_L1) or 12 min for longer chains (SiO_2@PDMAEMA_L2). The particles were collected by centrifugation at 12000 rpm for 10 min, washed 2 times in DMF and 3 times in ethanol and dried under vacuum at 25°C overnight.

4.10.2 | Ag@PDMAEMA

First, ligand exchange was used to introduce Br-initiator groups on silver particles by adding 300 μL Br-initiator (11-Sulfanylundecyl 2-bromo-2-methylpropanoate) to 200 mg silver particles well dispersed in 100 mL ethanol. After stirring for 12 h, the Ag@Br-initiator was collected by centrifugation and washed three times with 30 mL ethanol. Finally, Ag@Br-initiator was dispersed in 10 mL DMF and stored in the refrigerator. For variation of grafting density, 2-mercaptoethanol was used as a "dummy-initiator" and mixed with Br-initiator in different ratios. In this study, Br-initiator amount of 10%, 25%, 50%, and 100% was investigated.

Polymerization of PDMAEMA on silver surface was performed in DMF at 70°C in an oil bath for 60 min. Therefore, 50 mg Ag@Br-initiator particles, DMAEMA, 2 mL anhydrous DMF, 0.03 μL EBIB, 6 μL $CuBr_2$ (0.1 M solution in DMF), and 1.3 mg TPMA were added to a reaction tube with a stir bar, then the tube was sealed with a rubber septum and purged with argon and sonicated (80 W) in an ice-water bath for 10 min. Five systems with DMAEMA monomer concentrations of 0.28, 0.99, 1.7, 2.2, and 2.6 M were synthesized for variation of the resulting chain length (Ag@PDMAEMA_L1L5). Therefore, 0.1, 0.4, 0.8, 1.2, or 1.6 mL monomer were added, respectively, to the reaction mixture. Afterwards, 20 μL Sn(II)2ethylhexanoate dissolved in 0.2 mL DMF was injected. After the reaction, the particles were collected by centrifugation at 4000 rpm for 20 min, washed 2 times in 30 mL DMF and 3 times in 30 mL ethanol, and dispersed in 10 mL ethanol.

4.11 | In Situ Synthesis of Silver/Gold Nanoparticles in Polymer Brushes (Preparation of SiO_2-PDMAEMA@Ag, SiO_2-PDMAEMA@Au)

A total of 50 mg SiO_2-PDMAEMA particles (ø = 200 nm), 10 mL 80 mM $AgNO_3$ ($HAuCl_4$) aqueous solution were added to the test tube, the tube was sealed with a rubber septum and purged with argon and sonicated (80 W) in an ice-water bath for 30 min. Afterwards, 1 mL 0.05 M $NaBH_4$ was added dropwise with stirring at 500 rpm, the reaction lasted for 1 h. The particles were collected by centrifugation at 12000 rpm for 10 min, washed five times in ethanol, and dried under vacuum at 25°C overnight.

4.12 | Electrical Conductivity Measurement

Electrical conductivity of the particle films made of the different hybrid particle systems was determined by four-point probe test

[25]. In order to prepare the test sample, we coated the obtained composite nanoparticles on a PC substrate with 2 electrodes. Finally, a layer of 1 mm thick sample (2 mm in length and 2 mm in width) was prepared. According to the measurement results, the conductivity can be calculated as [25b]

$$\sigma = \frac{I \cdot l}{V \cdot d \cdot h}$$

where I is the current, V is the voltage across the electrodes, l is the distance between the two electrodes for voltage measurement, d is the width of the sample, and h is the thickness of the sample.

4.13 | Immobilization of Laccase

First, the acetate buffer solution (NaAc, 10 mM, pH 4.0) was prepared, then 10 mg grafted particles were dispersed in 3 mL buffer solution by ultrasound until no particles were visible at the bottom of the centrifuge tube (about 1 min). After three washes with 3 mL buffer solution, the particles were dispersed again in 0.5 mL of buffer solution and mixed with 0.5 mL laccase (~50 U/mL in 10 mM NaAc buffer) The immobilization was carried out at room temperature for 1 h under gentle shaking. Afterwards, the particles were washed with buffer solution until no activity was observed in the supernatant. Enzyme loading was quantified using TGA by calculating the difference in organic content before and after enzyme immobilization. Additionally, the decrease in laccase concentration in the supernatant was monitored by UV–Vis absorbance at 280 nm, using a standard calibration curve. These values were used to calculate the amount of enzyme immobilized per mg particle and allowed the calculation of the catalytic activity per mg polymer and mg immobilized enzyme.

4.14 | Determination of Enzyme Activity/Catalytic Activity

Determination of enzyme activity was performed with a Tristar 5 Multimode Plate Reader (Berthold Technologies). Laccase oxidizes 2,2′-azino-bis(3-ethylbenzothiazoline-6-sulfonic acid) (ABTS) to the green-colored cation-radical $ABTS^+$. 10 µL of the enzyme containing solution were added to 965 µL NaAc buffer solution (10 mM, pH 4) in the measurement well. During measurement 25 µL of 2 mM ABTS solution were added. Colorimetric changes were measured by absorbance spectroscopy at 420 nm. For the measurement of the change in absorbance (ΔE) within a particular time interval (Δt), the activity can be calculated by Equation (1), where Δt is the change in time, d is the path length trough the sample and ε is the extinction coefficient for the oxidation of ABTS at 420 nm ($36\,mM^{-1}\,cm^{-1}$).

$$\text{Activity} = \frac{\Delta E / \Delta t}{\varepsilon \cdot d} \quad (1)$$

For samples with high enzyme concentration, the solutions were diluted with NaAc buffer (pH 4; 1:10) before the ABTS assay was performed and activity calculated with respect to the dilution factor.

The enzyme solution used for immobilization as well as the supernatants obtained during the washing steps after enzyme immobilization were tested with the ABTS assay.

The efficiency of enzyme immobilization is determined by calculating the ratio of the enzymatic activity measured on particles with immobilized laccase and the activity of free laccase before immobilization (Equation 2):

$$\text{Enzyme Immobilization Efficiency [\%]} = \frac{\text{activity of immobilized laccase on particles}}{\text{initial activity of added free laccase}} \times 100\% \quad (2)$$

$$\text{Activity}\left(\frac{U}{\text{mg particle or polymer}}\right) = \frac{\text{Activity of immobilized enzyme}}{\text{mass of particle or polymer}} \quad (3)$$

Acknowledgments

The authors thank Ms. Kerstin Arnhold from Leibniz-Institut für Polymerforschung Dresden e. V. for GPC measurements. The authors would like to acknowledge the project funding from BMBF (FKZ: 031B1118B) and DFG (Grant SY125/15-1).

Conflicts of Interest

The authors declare no conflicts of interest.

References

1. (a) C. Marschelke, I. Raguzin, A. Matura, A. Fery, and A. Synytska, "Controlled and Tunable Design of Polymer Interface for Immobilization of Enzymes: Does Curvature Matter?," *Soft Matter* 13 (2017): 1074–1084. (b) C. Marschelke, M. Muller, D. Kopke, A. Matura, M. Sallat, and A. Synytska, "Hairy Particles With Immobilized Enzymes: Impact of Particle Topology on the Catalytic Activity," *ACS Applied Materials & Interfaces* 11 (2019): 1645–1654.

2. (a) S. T. Ten, U. Hashim, S. C. B. Gopinath, et al., "Highly Sensitive Escherichia Coli Shear Horizontal Surface Acoustic Wave Biosensor With Silicon Dioxide Nanostructures," *Biosensors & Bioelectronics* 93 (2017): 146–154. (b) Y. Wang, F. Qu, J. Liu, Y. Wang, J. Zhou, and S. Ruan, "Enhanced H2S Sensing Characteristics of CuO-NiO Core-Shell Microspheres Sensors," *Sensors and Actuators B: Chemical* 209 (2015): 515–523. (c) R. Frost, C. Wadell, A. Hellman, et al., "Core–Shell Nanoplasmonic Sensing for Characterization of Biocorona Formation and Nanoparticle Surface Interactions," *ACS Sensors* 1 (2016): 798–806. (d) Z. Li, X. Huang, H. Liu, et al., "Electrochemiluminescence Biosensor for Hyaluronidase Based on the Adjustable Electrostatic Interaction Between the Surface-Charge-Controllable Nanoparticles and Negatively Charged Electrode," *ACS Sensors* 7 (2022): 2012–2019. (e) X. Lu, G. Zhou, J. Zhang, et al., "Highly Sensitive Determination of 2,4,6-Trichlorophenol by Using a Novel SiO_2@MIPIL Fluorescence Sensor With a Double Recognition Functional Monomer," *ACS Sensors* 5 (2020): 1445–1454. (f) S. Bilge, B. Dogan-Topal, M. M. Gürbüz, S. A. Ozkan, and A. Sınağ, "Recent Trends in Core/Shell Nanoparticles: Their Enzyme-Based Electrochemical Biosensor Applications," *Microchimica Acta* 191 (2024): 240.

3. F. Zhao, J. Zeng, M. M. Parvez Arnob, et al., "Monolithic NPG Nanoparticles With Large Surface Area, Tunable Plasmonics, and High-Density Internal Hot-Spots," *Nanoscale* 6 (2014): 8199–8207.

4. Y. Xu, Y. Qin, S. Palchoudhury, and Y. Bao, "Water-Soluble Iron Oxide Nanoparticles With High Stability and Selective Surface Functionality," *Langmuir* 27 (2011): 8990–8997.

5. Y. Mei, G. Sharma, Y. Lu, et al., "High Catalytic Activity of Platinum Nanoparticles Immobilized on Spherical Polyelectrolyte Brushes," *Langmuir* 21 (2005): 12229–12234.

6. (a) K. M. Yeon, J. You, M. D. Adhikari, et al., "Enzyme-Immobilized Chitosan Nanoparticles as Environmentally Friendly and Highly Effective Antimicrobial Agents," *Biomacromolecules* 20 (2019): 2477–2485. (b) Y. Xu, F. Y. H. Kutsanedzie, M. Hassan, et al., "Mesoporous Silica Supported Orderly-Spaced Gold Nanoparticles SERS-Based Sensor for Pesticides Detection in Food," *Food Chemistry* 315 (2020): 126300. (c) Q. Li, J.-j. Liu, X. Sun, and L. Xu, "Hierarchically Porous Melamine-Formaldehyde Resin Microspheres for the Removal of Nanoparticles and Simultaneously as the Nanoparticle Immobilized Carrier for Catalysis," *ACS Sustainable Chemistry & Engineering* 7 (2018): 867–876.

7. S. Berger, A. Synytska, L. Ionov, K. J. Eichhorn, and M. Stamm, "Stimuli-Responsive Bicomponent Polymer Janus Particles by "Grafting From"/"Grafting to" Approaches," *Macromolecules* 41 (2008): 9669–9676.

8. A. Synytska, E. Svetushkina, N. Puretskiy, et al., "Biocompatible Polymeric Materials With Switchable Adhesion Properties," *Soft Matter* 6 (2010): 5907–5914.

9. O. Azzaroni, S. Moya, T. Farhan, A. A. Brown, and W. T. S. Huck, "Switching the Properties of Polyelectrolyte Brushes via "Hydrophobic Collapse"," *Macromolecules* 38 (2005): 10192–10199.

10. (a) H.-C. Lin, C.-C. Li, and J.-T. Lee, "Nitroxide Polymer Brushes Grafted Onto Silica Nanoparticles as Cathodes for Organic Radical Batteries," *Journal of Power Sources* 196 (2011): 8098–8103. (b) K.-u.-R. Naveed, L. Wang, H. Yu, et al., "Synthesis of Poly(Diethylaminoethyl Methacrylate-Co-2,2,6,6-Tetramethyl-4-Piperidyl Methacrylate)s and Their Segmental Motion Study," *Colloid and Polymer Science* 298 (2020): 1473–1486.

11. D. X. Li, Q. He, Y. Cui, and J. B. Li, "Fabrication of pH-Responsive Nanocomposites of Gold Nanoparticles/Poly(4-Vinylpyridine)," *Chemistry of Materials* 19 (2007): 412–417.

12. B. Liu, W. Zhang, F. Yang, H. Feng, and X. Yang, "Facile Method for Synthesis of Fe3O4@Polymer Microspheres and Their Application as Magnetic Support for Loading Metal Nanoparticles," *Journal of Physical Chemistry C* 115 (2011): 15875–15884.

13. (a) E. B. Aydın, M. Aydın, and M. K. Sezgintürk, "Determination of Calreticulin Using Fe3O4@AuNPs Core-Shell Functionalized With PT(COOH)2 Polymer Modified Electrode: A New Platform for the Impedimetric Biosensing of Cancer Biomarkers," *Sensors and Actuators B: Chemical* 367 (2022): 132099. (b) D. Yu, Y. Zeng, Y. Qi, T. Zhou, and G. Shi, "A Novel Electrochemical Sensor for Determination of Dopamine Based on AuNPs@SiO_2 Core-Shell Imprinted Composite," *Biosensors & Bioelectronics* 38 (2012): 270–277. (c) T. Feng, K. Chen, J. Zhong, Y. Cheng, H. Zhao, and M. Lan, "In-Situ Polymerization of Dendritic Polyaniline Nanofibers Network Embedded With Ag@SiO_2 Core-Shell Nanoparticles for Electrochemical Determination of Trace Arsenic(III)," *Sensors and Actuators B: Chemical* 369 (2022): 132265.

14. L. Yang, S. Liu, Q. Zhang, and F. Li, "Simultaneous Electrochemical Determination of Dopamine and Ascorbic Acid Using AuNPs@Polyaniline Core–Shell Nanocomposites Modified Electrode," *Talanta* 89 (2012): 136–141.

15. (a) Z. Farka, T. Jurik, D. Kovar, L. Trnkova, and P. Skladal, "Nanoparticle-Based Immunochemical Biosensors and Assays: Recent Advances and Challenges," *Chemical Reviews* 117 (2017): 9973–10042. (b) N. Wongkaew, M. Simsek, C. Griesche, and A. J. Baeumner, "Functional Nanomaterials and Nanostructures Enhancing Electrochemical Biosensors and Lab-On-a-Chip Performances: Recent Progress, Applications, and Future Perspective," *Chemical Reviews* 119 (2019): 120–194. (c) J. Kaltbeitzel and P. R. Wich, "Protein-Based Nanoparticles: From Drug Delivery to Imaging, Nanocatalysis and Protein Therapy," *Angewandte Chemie (International Ed. in English)* 62 (2023): e202216097.

16. S. Lee, A. M. Gonzalez-Suarez, X. Huang, et al., "Using Electrochemical Immunoassay in a Novel Microtiter Plate to Detect Surface Markers of Preeclampsia on Urinary Extracellular Vesicles," *ACS Sensors* 8 (2023): 207–217.

17. L. Bayne, R. V. Ulijn, and P. J. Halling, "Effect of Pore Size on the Performance of Immobilised Enzymes," *Chemical Society Reviews* 42 (2013): 9000–9010.

18. X. Wang, J. Shi, S. Zhang, et al., "MOF-Templated Rough, Ultrathin Inorganic Microcapsules for Enzyme Immobilization," *Journal of Materials Chemistry B* 3 (2015): 6587–6598.

19. Y. Lu, Y. Mei, M. Drechsler, and M. Ballauff, "Thermosensitive Core–Shell Particles as Carriers for Ag Nanoparticles: Modulating the Catalytic Activity by a Phase Transition in Networks," *Angewandte Chemie (International Ed. in English)* 45 (2006): 813–816.

20. M. Peixoto de Almeida, P. Quaresma, S. Sousa, et al., "Measurement of Adsorption Constants of Laccase on Gold Nanoparticles to Evaluate the Enhancement in Enzyme Activity of Adsorbed Laccase," *Physical Chemistry Chemical Physics* 20 (2018): 16761–16769.

21. X. Liu, Y. Yin, and C. Gao, "Size-Tailored Synthesis of Silver Quasi-Nanospheres by Kinetically Controlled Seeded Growth," *Langmuir* 29 (2013): 10559–10565.

22. L. Chang, H. X. Yan, J. Chang, and J. E. Gautrot, "Cationic Polymer Brush-Coated Bioglass Nanoparticles for the Design of Bioresorbable RNA Delivery Vectors," *European Polymer Journal* 156 (2021): 1–9.

23. C. Marschelke, M. Müller, D. Köpke, A. Matura, M. Sallat, and A. Synytska, "Hairy Particles With Immobilized Enzymes: Impact of Particle Topology on the Catalytic Activity," *ACS Applied Materials & Interfaces* 11 (2019): 1645–1654.

24. J. C. Conrad and M. L. Robertson, "Shaping the Structure and Response of Surface-Grafted Polymer Brushes via the Molecular Weight Distribution," *JACS Au* 3 (2023): 333–343.

25. (a) L. Sun, J. Wang, and E. Bonaccurso, "Conductivity of Individual Particles Measured by a Microscopic Four-Point-Probe Method," *Scientific Reports* 3 (2013): 1991. (b) H. Yuk, B. Lu, S. Lin, et al., "3D Printing of Conducting Polymers," *Nature Communications* 11 (2020): 1604.

Supporting Information

Additional supporting information can be found online in the Supporting Information section.